# Landau theory and giant room-temperature barocaloric effect in $MF_3$ metal trifluorides

A. Corrales-Salazar,[1] R. T. Brierley,[2] P. B. Littlewood,[3,4] and G. G. Guzmán-Verri[1,4]
[1]*Centro de Investigación en Ciencia e Ingeniería de Materiales and Escuela de Física, Universidad de Costa Rica, San José, Costa Rica 11501*
[2]*Department of Physics, Yale University, New Haven, Connecticut 06511, USA*
[3]*James Franck Institute, University of Chicago, 929 E. 57 St., Chicago, Illinois 60637, USA*
[4]*Materials Science Division, Argonne National Laboratory, Argonne, Illinois 60439, USA*
(Received 3 August 2017; published 17 October 2017)

The structural phase transitions of $MF_3$ ($M$ = Al, Cr, V, Fe, Ti, Sc) metal trifluorides are studied within a simple Landau theory consisting of tilts of rigid $MF_6$ octahedra associated with soft antiferrodistortive optic modes that are coupled to long-wavelength strain generating acoustic phonons. We calculate the temperature and pressure dependence of several quantities such as the spontaneous distortions, volume expansion, and shear strains as well as $T - P$ phase diagrams. By contrasting our model to experiments we quantify the deviations from mean-field behavior and find that the tilt fluctuations of the $MF_6$ octahedra increase with metal cation size. We apply our model to predict giant barocaloric effects in Sc-substituted $TiF_3$ of up to about 15 J K$^{-1}$ kg$^{-1}$ for modest hydrostatic compressions of 0.2 GPa. The effect extends over a wide temperature range of over 140 K (including room temperature) due to a large predicted rate, $dT_c/dP = 723$ K GPa$^{-1}$, which exceeds those of typical barocaloric materials. Our results suggest that open lattice frameworks such as the trifluorides are an attractive platform to search for giant barocaloric effects.

DOI: 10.1103/PhysRevMaterials.1.053601

## I. INTRODUCTION

Metal trifluorides (or simply trifluorides) are a class of materials with chemical formula $MF_3$ ($M$ = Al, Cr, V, Fe, Ti, Sc) and with an open lattice framework in which the trivalent metal ion $M$ is surrounded by an octahedron of corner-shared fluorine atoms [1,2]. They are isostructural to $ReO_3$, a well-known $ABO_3$ perovskite in which the $A$ site is vacant [3]. They can exhibit large thermal expansion (TE) which can be reversibly tuned from positive (PTE) to negative (NTE) by temperature, pressure, cation substitution, or redox intercalation [4–10]. This makes the trifluorides attractive for designing materials that are dimensionally stable and resistant to thermal shocks [11].

At ambient pressure, most trifluorides exhibit antiferrodistortive structural transitions with cubic-to-rhombohedral (c-r) transformations in which the $MF_6$ octahedron tilts around the (111) axis. The tilting angles are large, e.g., about 14° in $AlF_3$ at room temperature (RT) [12], and are accompanied by spontaneous shear and volume strains [13]. Such lattice instability is the result of the condensation of a threefold zone-boundary $R_4^+$ phonon mode of the cubic phase located at the wave vector $(1,1,1)(\pi/a)$ [14]. Below the transition, the $R_4^+$ mode splits into a low-energy $E_g$ doublet and a high energy $A_{1g}$ singlet [15].

Density functional theory [14], molecular dynamics (MD) simulations [16], and electrostatic energy considerations [17] have shown that the driving force of the lattice instability in the trifluoride is of dipolar origin. When the $M$-F-$M$ bond bends, fluorine displaces transverse to the bond length, generating an electric dipole with a negative end at the $F^-$ anion and a positive end at its cubic lattice site. This distortion concomitantly induces a polarization in the fluorine electron cloud that is opposite to the displacive dipole. While there is an energy penalty for creating such induced dipoles, the resulting interactions between the induced dipoles and between the induced dipoles with the ionic charges lower the total energy to favor the $r$ phase over the parent $c$ structure preferred by the purely ionic Madelung energy.

A trifluoride of special recent interest is $ScF_3$, an ionic insulator with a wide indirect energy band gap of about 8–10 eV [18]. It does not have a structural transition to an $r$ phase at ambient pressure but rather exhibits incipient behavior in which a nearly flat $M$-$R$ phonon branch softens without condensing, as it has been observed by inelastic x-ray scattering experiments (IXS) [19] and found in *ab initio* calculations [20]. It exhibits strong negative TE (−34 ppm K$^{-1}$ near RT) from 10 to 1100 K [21] and very strong lattice anharmonicities (its soft $R_4^+$ mode is described by a quartic potential energy in the tilts) [22]. Its incipient behavior and proximity to an $r$ phase induced by, e.g., cation substitution [4,5,7] suggest that $ScF_3$ is one of the few known stoichiometric materials near a quantum structural phase transition [19].

With hydrostatic compression, the $r$ phase can be induced at higher temperatures. For example, at about 0.6 GPa, a $c$-$r$ transition is observed near RT in the incipient $ScF_3$ [21,23,24]. X-ray diffraction experiments have determined the temperature-pressure phase diagrams for Sc-substituted $AlF_3$($Sc_{1-x}Al_xF_3$) [7]. Very significantly, they have observed linearly increasing transition temperatures with pressure with large rates ($dT_c/dP \simeq$ 400–500 K GPa$^{-1}$) that vary little with Sc concentration and pressure [7,21]. Additional pressure-induced transitions have been reported at higher pressures [23,24].

While microscopic models for the trifluoride are available [14,16,17], there is currently no macroscopic approach based on the simple Landau phenomenology. The purpose of this work is thus to construct such a theory. Our model consists of rigid tilts of the $MF_6$ octahedra associated with the soft $R_4^+$ optic mode coupled to long-wavelength strain generating acoustic phonons. The model is similar to those used to describe the widely studied antiferrodistortive transitions of $SrTiO_3$ and $LaAlO_3$ [25,26], but with the important

 

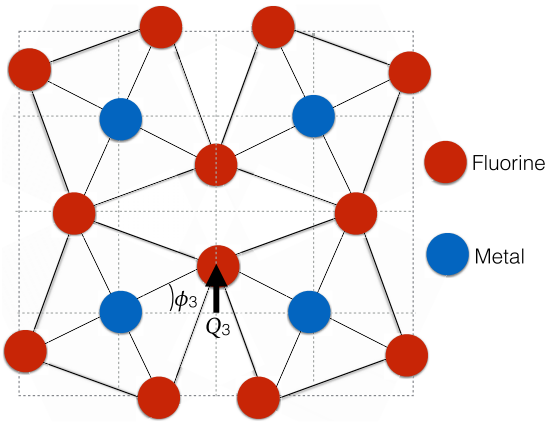


FIG. 1. A (001) section of the $MF_3$ lattice illustrating the displacement of fluorine ions described by the soft-mode coordinate $Q_3$ and the antiferrodistortive rotation $\phi_3$ of the $MF_6$ octahedra at around (001).

distinctions that in the trifluorides the phase transition can be discontinuous and that there are large excess volume strains. By comparing our model to experiments on several trifluorides, we quantify the deviations from mean-field behavior and found trends with the metal cation size.

We also apply our model to predict the barocaloric effect (BCE) in the trifluorides. BCEs are reversible thermal changes in a substance in response to changes in hydrostatic pressure and are currently of enormous interest for their potential in developing clean and efficient solid-state cooling technologies [27]. It is expected that materials with strong TE such as the trifluorides should give rise to large barocaloric responses, as their entropy rate $(\partial S/\partial P)_T = -(\partial V/\partial T)_P$, according to the Maxwell's relations [27]. Indeed, we show that the isothermal changes entropy in the trifluorides are comparable to those of other classes of materials exhibiting so-called giant BCEs [28–36] and that it can extend over a broad temperature range which includes RT for modest changes in pressure as a result of their large barocaloric coefficients $dT_c/dP$. So far, the BCE in the trifluoride has not been studied neither experimentally nor theoretically.

This paper is organized as follows: In Sec. II we present our Landau theory to describe the structural transitions; in Sec. III we show our results and discussion, including a comparison to the isostructural compounds $ReO_3$ and $WO_3$; and in Sec. IV we present our conclusions.

## II. LANDAU THEORY

### A. Free energy

We choose the order parameter as the linear displacement $\boldsymbol{Q} = (Q_1, Q_2, Q_3)$, which represents, in first order, an antiferrodistortive rotation of the $MF_6$ octahedra through angles $\phi_i$ and $-\phi_i, (i = 1,2,3)$ about axes parallel to a cube edge. We normalize the $Q's$ in such a way that they are numerically equal to the linear fluorine displacements. They are related to $\phi_i$ by $\tan\phi_i = 2Q_i/a$, where $a$ is the lattice constant, see Fig. 1. In addition to the antiferrodistortive distortion, we introduce elastic strains $\eta_\alpha$ as a secondary order parameter. We write the components of the strain tensor in the usual Voigt notation: $\eta_\alpha \equiv \epsilon_{\alpha\alpha} = \partial u_\alpha/\partial x_\alpha (\alpha = 1,2,3)$, $\eta_4 = 2\epsilon_{yz} = 2(\partial u_y/\partial z + \partial u_z/\partial y), \eta_5 = 2\epsilon_{xz} = 2(\partial u_x/\partial z + \partial u_z/\partial x)$, and $\eta_6 = 2\epsilon_{xy} = 2(\partial u_x/\partial y + \partial u_y/\partial x)$. We do not consider fluctuations in $\boldsymbol{Q}$ and $\eta_\alpha$.

Our Landau free energy density is given as follows:

$$G_Q + G_\eta + P\sum_{\alpha=1}^{3}\eta_\alpha, \tag{1}$$

where $G_Q$ is a strain-free free energy,

$$\begin{aligned} G_Q = G_0 &+ \frac{A}{2}\left(Q_1^2 + Q_2^2 + Q_3^2\right) \\ &+ \frac{u}{2}\left(Q_1^2+Q_2^2+Q_3^2\right)^2 + \frac{3v}{2}\left(Q_1^2Q_2^2 + Q_1^2Q_3^2 + Q_2^2Q_3^2\right) \\ &+ \frac{w_1}{6}\left(Q_1^2 + Q_2^2 + Q_3^2\right)^3, \end{aligned} \tag{2}$$

where $A = A_0(T - T_0)$ and $T_0$ is the supercooling temperature that limits of stability of the parent $c$ phase. $G_\eta$ is an energy density with elastic couplings,

$$\begin{aligned} G_\eta = {} & e_a(\eta_1 + \eta_2 + \eta_3)\left(Q_1^2 + Q_2^2 + Q_3^2\right) \\ & - e_t\left[\eta_1\left(2Q_1^2 - Q_2^2 - Q_3^2\right) + \eta_2\left(2Q_2^2 - Q_1^2 - Q_3^2\right)\right. \\ & \left. + \eta_3\left(2Q_3^2 - Q_1^2 - Q_2^2\right)\right] \\ & - e_r(Q_1Q_2\eta_6 + Q_1Q_3\eta_5 + Q_2Q_3\eta_4) + \frac{1}{2}\sum_{\alpha\beta} C^0_{\alpha\beta}\eta_\alpha\eta_\beta. \end{aligned} \tag{3}$$

$A_0, u, v, w, e_a, e_t$, and $e_r$ are model parameters independent of temperature and pressure, and $C^0_{\alpha\beta}$ are the usual elastic constants of the parent phase in the Voigt notation. The third term in the free energy (1) is a hydrostatic compression where $P$ is measured from atmospheric pressure.

In writing the free energy (1), we have not considered any polar degrees of freedom associated with phonon modes that break inversion symmetry as there is no evidence that such lattice modes are unstable in the trifluorides, e.g., the zone-center TO phonon modes do not condense and remain fairly energetic, such as in $ScF_3$ (4–5 THz) [20,37,38] and other trifluorides [39]. Moreover, Clausius-Mossotti theory predicts that the ground state exhibits antipolar order from the $MF_6$ tilts with null polarization [17]. We have also ignored sixth-order cubic anisotropies. Our results will show that this is justified as long as we are describing the $r$ phase. In Appendix B, we show, however, that they are essential to describe other pressure-induced phases. We have also neglected any polar degrees of freedom associated with phonon modes that would break inversion symmetry, as there is no evidence that such lattice modes are unstable in the trifluorides.

Minimizing Eq. (1) with respect to the strains gives

$$\begin{aligned} \eta_1 &= -\frac{e_a}{3C_a}\left(Q_1^2 + Q_2^2 + Q_3^2\right) \\ &\quad + \frac{e_t}{2C_t}\left(2Q_1^2 - Q_2^2 - Q_3^2\right) - \frac{P}{3C_a}, \\ \eta_2 &= -\frac{e_a}{3C_a}\left(Q_1^2 + Q_2^2 + Q_3^2\right) \end{aligned}$$

$$+\frac{e_t}{2C_t}\left(2Q_2^2-Q_1^2-Q_3^2\right)-\frac{P}{3C_a},$$

$$\eta_3=-\frac{e_a}{3C_a}\left(Q_1^2+Q_2^2+Q_3^2\right)$$

$$+\frac{e_t}{2C_t}\left(2Q_3^2-Q_1^2-Q_2^2\right)-\frac{P}{3C_a},$$

$$\eta_4=\frac{e_r}{C_r}Q_2Q_3,$$

$$\eta_5=\frac{e_r}{C_r}Q_1Q_3,$$

$$\eta_6=\frac{e_r}{C_r}Q_1Q_2, \tag{4}$$

where $C_a=(1/3)(C_{11}^0+2C_{12}^0)$ is the bulk modulus, $C_t=(1/2)(C_{11}^0-C_{12}^0)$, and $C_r=C_{44}^0$ are the shear tetragonal and rhombohedral moduli, respectively.

When the spontaneous strains of Eq. (4) are substituted back into Eq. (1), we obtain, as expected [25], that the free energy has the same form as that of Eq. (2) for the strain-free case, except with renormalized quadratic ($A$) and quartic coefficients ($u$ and $v$) and a uniform energy shift due to pressure:

$$\tilde{G}(T,P)=G_0+\frac{1}{2}\tilde{A}\left(Q_1^2+Q_2^2+Q_3^2\right)+\frac{\tilde{u}}{2}\left(Q_1^2+Q_2^2+Q_3^2\right)^2$$

$$+\frac{3\tilde{v}}{2}\left(Q_1^2Q_2^2+Q_1^2Q_3^2+Q_2^2Q_3^2\right)$$

$$+\frac{w_1}{6}\left(Q_1^2+Q_2^2+Q_3^2\right)^3-\frac{1}{2}\frac{P^2}{C_a}, \tag{5}$$

where

$$\tilde{A}=A-\frac{2e_aP}{C_a}, \tag{6}$$

and

$$\tilde{u}=u-\left(5\frac{e_a^2}{C_a}+3\frac{e_t^2}{C_t}\right), \tag{7a}$$

$$\tilde{v}=v+\left(3\frac{e_t^2}{C_t}-\frac{1}{3}\frac{e_r^2}{C_r}\right). \tag{7b}$$

We conclude the presentation of the free energy here. In the next section we apply our model to describe the $c$-$r$ transition of the trifluorides.

### B. $c$-$r$ transition

The symmetry of the ground state and order of the phase transition is determined by the choice of $\tilde{u}$ and $\tilde{v}$. For a $c$-$r$ discontinuous (continuous) transition, we must have $\tilde{v}<0$ and $\tilde{u}+\tilde{v}<0$ ($\tilde{u}+\tilde{v}>0$) [25].

To describe the $r$ phase, we take $\boldsymbol{Q}=(Q_s/\sqrt{3})(1,1,1)$, where $Q_s$ is determined by minimization of the free energy (5),

$$Q_s(T,P)=\pm\left\{\sqrt{\left(\frac{\tilde{u}+\tilde{v}}{w_1}\right)^2-\frac{\tilde{A}}{w_1}}-\left(\frac{\tilde{u}+\tilde{v}}{w_1}\right)\right\}^{1/2}. \tag{8}$$

Substitution of the order parameter (8) into Eq. (4) gives, respectively, the following the spontaneous volume and shear strains:

$$\eta_a=\eta_1+\eta_2+\eta_3=-\frac{e_a}{C_a}Q_s^2-P/C_a, \tag{9a}$$

$$\eta_r=\eta_4=\eta_5=\eta_6=\frac{e_r}{3C_r}Q_s^2=\cos\alpha_C, \tag{9b}$$

where $\alpha_C$ as the angle between any two axes of the $c$-unit cell.

Experiments [5,7,12] usually report the ratio between the lattice constants $c_H$ and $a_H$ of a hexagonal unit cell as

$$\frac{c_H}{a_H}=\sqrt{\frac{3}{2}\frac{1+2\cos\alpha_R}{1-\cos\alpha_R}}, \tag{10}$$

where $\alpha_R$ is the angle between any two vectors of an $r$ unit cell. $\alpha_R$ and $\alpha_C$ are related as follows:

$$\cos\alpha_R=\frac{1}{2}\frac{1+3\cos\alpha_C}{1+\cos\alpha_C}. \tag{11}$$

We now derive expressions for the relevant temperature scales. From $Q_s$ of Eq. (8), we find that the stability of the $r$ phase ends at the superheating temperature,

$$T^*(P)=T^*(0)+\left(\frac{2}{A_0}\frac{e_a}{C_a}\right)P, \tag{12}$$

where $T^*(0)=T_0+\frac{w_1}{A_0}\left(\frac{\tilde{u}+\tilde{v}}{w_1}\right)^2$ is the superheating temperature at ambient pressure. By equating the free energies $\tilde{G_Q}$ of the high- and low-temperature phases, we find the transition temperature

$$T_c(P)=T_c(0)+\left(\frac{2}{A_0}\frac{e_a}{C_a}\right)P, \tag{13}$$

where $T_c(0)=T_0+\frac{3}{4}\frac{w_1}{A_0}\left(\frac{\tilde{u}+\tilde{v}}{w_1}\right)^2$ is the transition temperature at ambient pressure. In the next sections, we calculate several thermodynamic quantities of interest.

#### *Coefficient of thermal expansion, entropy, latent heat, heat capacity, and barocaloric effect*

We begin with the volume change with temperature and the coefficient of thermal expansion (CTE). The temperature and pressure dependence of the volume $V$ is given by [40]

$$V(T)/V_0=\frac{\partial\tilde{G}}{\partial P}=\begin{cases}1-\frac{P}{C_a}, & T>T_c\\ 1-\frac{e_a}{C_a}Q_s^2-\frac{P}{C_a}, & T<T_c.\end{cases} \tag{14}$$

$V_0$ is a reference volume and $(\partial G_0/\partial P)=1$. As expected, the relative change in volume in the $r$ phase is equal to the volumetric strain $\eta_1+\eta_2+\eta_2$. The CTE is given as follows:

$$\kappa(T)=\frac{\partial^2\tilde{G}}{\partial T\partial P},$$

$$=\begin{cases}(\partial V_0/\partial T)=\kappa_0, & T>T_c\\ \kappa_0+\frac{1}{2}\frac{e_a}{C_a}\frac{A_0/w_1}{\sqrt{\left(\frac{\tilde{u}+\tilde{v}}{w_1}\right)^2-\frac{\tilde{A}}{w_1}}}, & T<T_c.\end{cases} \tag{15}$$

We calculate the entropy per unit volume from the free energy of Eq. (5),

$$S(T,P) = -\frac{\partial \tilde{G}}{\partial T} = \begin{cases} S_0, & T > T_c, \\ S_0 - \frac{A_0}{2} Q_s^2, & T < T_c. \end{cases} \quad (16)$$

The latent heat per unit volume of the transition at $P = 0$ is then given as follows:

$$T_c \Delta S(T_c,0) = T_c \times \frac{A_0}{2} Q_s^2(T_c,0), \quad (17)$$

where $\Delta S(T_c,0)$ is the entropy jump at the $c$-$r$ transition.

We now calculate the heat capacity per unit volume,

$$C_P = T\frac{\partial S(T,P)}{\partial T} = \begin{cases} C_P^0, & T > T_c, \\ C_P^0 + T\frac{A_0}{4}\frac{A_0/w_1}{\sqrt{\left(\frac{\tilde{u}+\tilde{v}}{w_1}\right)^2 - \frac{\tilde{A}}{w_1}}}, & T < T_c, \end{cases} \quad (18)$$

where $C_P^0 = T(\partial S_0/\partial T)$ is a reference heat capacity in the high-temperature phase.

From Eq. (16), we calculate the isotropic changes in entropy,

$$\Delta S(T,P) = \begin{cases} 0, & T > T_c, \\ -\frac{A_0}{2}\left[Q_s^2(T,P) - Q_s^2(T,0)\right], & T < T_c. \end{cases} \quad (19)$$

We conclude the presentation of our model here. In the next section we apply it to several trifluorides.

## III. RESULTS AND DISCUSSION

### A. Fits and comparison to experiments

We now discuss our fits to several trifluoride compounds. For pure $TiF_3$ and $AlF_3$, we fit our model to their observed $c_H/a_H$, $M$-F-$M$ bond angle, volume expansion, CTE, and latent heat of the transition [2,5,7,12], see Fig. 2. For $Sc_{1-x}Al_xF_3$ with $x < 1$, we do a slightly different fit since their latent heats are unknown: we fix the ratio $dT_c/dP = 2e_a/(A_0C_a)$ to that of the pure compound $AlF_3$. This is justified by the observed linear $T - P$ phase diagram of $Sc_{1-x}Al_xF_3$ with a slope that varies little with composition $x$ [7]. We do a similar fit for $Sc_{1-x}Ti_xF_3$. The resulting parameters together with the calculated supercooling and superheating temperatures are given in Table I.

Overall, we find that that there is good agreement between our model and experiments. The discrepancies between the observed and calculated $M$-F-$M$ bond angles above $T_c$ shown in Figs. 2(g) and 2(h) are due to local lattice distortions from the average $c$ structure [16,41], which we have not considered in our model. More importantly, the deviations from mean-field behavior are most noticeable in the volume expansions of $ScF_3$ and $AlF_3$ [see Figs. 2(c) and 2(d)], which correspond to the extreme cases of large and small metal-ion radius considered in this work ($r_{Sc} = 0.745$ Å, $r_{Al} = 0.535$ Å). This suggests a trend with $M$-cation size. In $ScF_3$, NTE is the result of cooperative tilt fluctuations of the rigid $ScF_6$ octahedra which reduce the average Sc-Sc distance while keeping the Sc-F distance fixed. Such fluctuations can only give rise to NTE; therefore the PTE in $AlF_3$ must originate from nonrigid modes

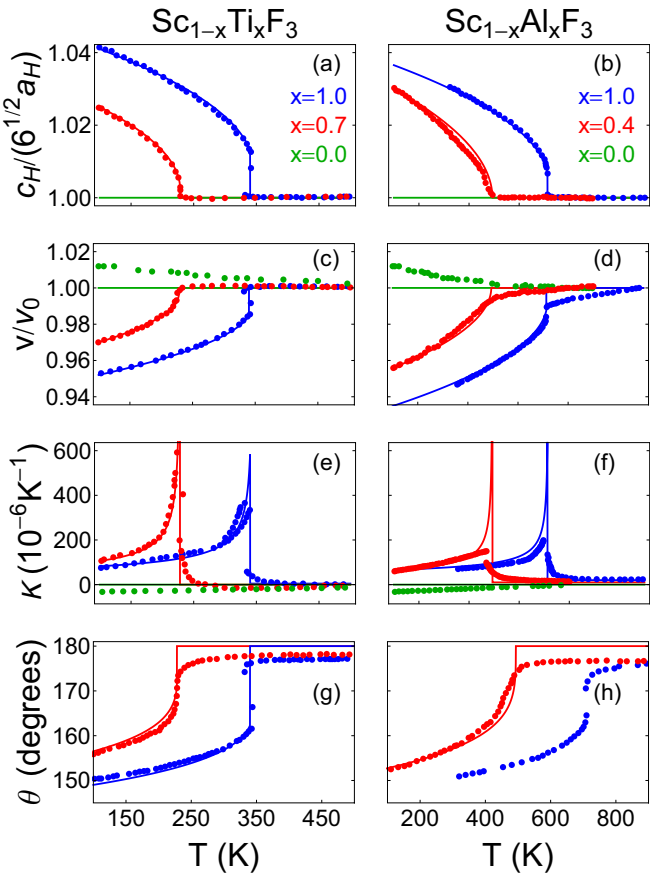


FIG. 2. Comparison between our model (solid line) and experiments (dots) for the temperature dependence of (a), (b) ratio hexagonal lattice constants, (c), (d) unit cell volume, (e), (f) CTE, and (g), (h) metal-F-metal bond angle $\theta$ in $Sc_{1-x}Ti_xF_3$ and $Sc_{1-x}Al_xF_3$. Data taken from Refs. [5,7,12].

such as Al-F bond stretching, which we have not considered in our model. $Sc_{1-x}Ti_xF_3$ with $x = 0.7$ has a mean B-site radius in between these two extremes (0.69 Å) and the deviations from our model and its observed volume expansion are tiny,

TABLE I. Model parameters for $Sc_{1-x}Al_xF_3$ and $Sc_{1-x}Ti_xF_3$ and predicted supercooling ($T_0$) and superheating ($T^*$) temperatures at ambient pressure. Transition temperatures ($T_c$) taken from Refs. [5,7,12].

| | $Sc_{1-x}Al_xF_3$ | | $Sc_{1-x}Ti_xF_3$ | |
|---|---|---|---|---|
| | $x = 1.0$, | $x = 0.4$ | $x = 1.0$, | $x = 0.7$ |
| $\kappa_0$ [$10^{-6}$ K$^{-1}$] | 10 | 10 | 0 | 0 |
| $\tilde{u} + \tilde{v}$ [meV Å$^{-7}$] | −0.78 | 0.05 | −0.81 | −0.27 |
| $A_0$ [$10^{-3}$ meV K$^{-1}$ Å$^{-5}$] | 3.7 | 5.8 | 2.9 | 3.1 |
| $w$ [meV Å$^{-9}$] | 12 | 48 | 13 | 17 |
| $e_a/C_a$ [Å$^{-2}$] | 0.13 | 0.20 | 0.17 | 0.17 |
| $e_r/C_r$ [Å$^{-2}$] | 0.14 | 0.27 | 0.28 | 0.30 |
| $T_0$ [K] | 703 | 493 | 327 | 227 |
| $T^*$ [K] | 718 | 493 | 344 | 228 |
| $T_c$ [K] | 713 | 493 | 340 | 228 |

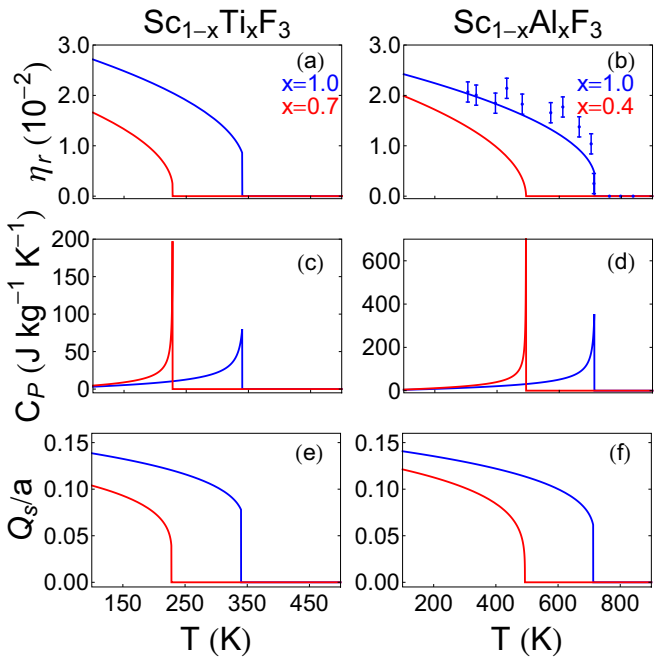


FIG. 3. (a), (b) Spontaneous shear strains, (c), (d) excess specific heat, and (e), (f) order parameter predicted from the fits obtained from Fig. 2 for $Sc_{1-x}Ti_xF_3$ and $Sc_{1-x}Al_xF_3$. Measured spontaneous strains (dots) taken from Ref. [13].

which indicates that the fluctuations of both rigid and nonrigid modes are unimportant. A picture therefore emerges in which rigid octahedra fluctuations dominate the TE for large metal ions and decrease with their size, while nonrigid vibrational modes dominate the TE for small metal ions and decrease with increasing radius.

Figure 3 shows the predicted spontaneous shear strains, order parameter, and specific heats for $Sc_{1-x}Al_xF_3$ and $Sc_{1-x}Ti_xF_3$ using our parametrization. Our prediction for the shear strains in $AlF_3$ compares well with experiments [13].

Figures 4(a) and 4(b) show the $T-P$ phase diagrams of $Sc_{1-x}Ti_xF_3$ and $Sc_{1-x}Al_xF_3$ calculated from Eq. (13). The linear dependence between $T$ and $P$ of our model agrees with the observed phase diagram for $Sc_{1-x}Al_xF_3$ [7,21]. Using Eq. (13) and the parameters from Table I, we find that $dT_c/dP \simeq 0.4 \times 10^3\,\mathrm{K\,GPa^{-1}}$, which is in excellent agreement with experiments [7,21]. For $Sc_{1-x}Ti_xF_3$, we predict that $dT_c/dP \simeq 0.7 \times 10^3\,\mathrm{K\,GPa^{-1}}$. There are no reports on the calculated or measured $T-P$ phase diagram for $Sc_{1-x}Ti_xF_3$ in the literature.

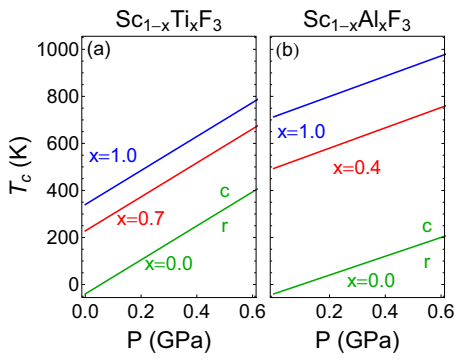


FIG. 4. Calculated $T-P$ phase diagrams for (a) $Sc_{1-x}Ti_xF_3$ and (b) $Sc_{1-x}Al_xF_3$.

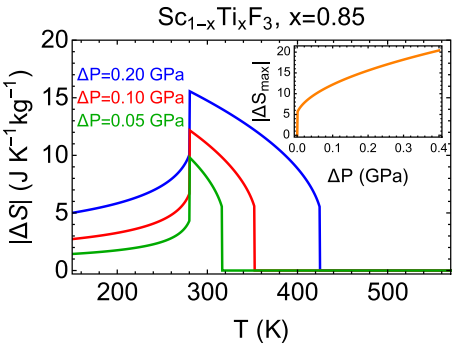


FIG. 5. Calculated isothermal changes in entropy for $Sc_{1-x}Ti_xF_3$, $x = 0.85$. Inset: Pressure dependence of the maximum changes in entropy.

In Appendix A, we derive expressions for the temperature dependence of the soft-mode frequencies. In the parent $c$ phase, we find the usual mean-field behavior for the $R_4^+$ mode, $\omega_{R_4^+} \propto \sqrt{A_0(T-T_0)}$, which is in agreement with IXS [19]. In addition, our values for $A_0$ given in Table I are about what is expected from the observed soft mode ($A_0 \simeq 3 \times 10^{-3}\,\mathrm{meV\,K^{-1}\,\AA^{-5}}$) for $ScF_3$ [19]. The temperature dependence of the $A_{1g}$ and $E_g$ phonon frequencies in the $r$ phase has been measured by Raman scattering experiments for $AlF_3$ [2]; however, we cannot compare to our model as the shear moduli $C_t$ and $C_r$ are unknown.

### B. Barocaloric effect

Figure 5 shows the predicted BCE for $Sc_{1-x}Ti_xF_3$ ($x = 0.85$) calculated from Eq. (19). We have chosen this composition as its $c$-$r$ transition occurs near room temperature ($T_c = 283$ K) and exhibits a strong first-order character [5]. As expected from the large CTEs, the resulting isothermal changes in entropy are comparable to those exhibiting giant effects [34], as it is shown in Table II. Moreover, the effect extends over a temperature range of about 140 K for pressure changes of 0.2 GPa, which includes RT. The wide temperature range is a consequence of the large predicted value of $dT_c/dP(=723\,\mathrm{K\,GPa^{-1}})$, which exceeds those of typical barocaloric compounds, see Table II. The inset in Fig. 5 shows the expected monotonic growth of maximum entropy changes at $T_c$, $\Delta S_{\max}$, with changes in pressure.

### C. Comparison to $ReO_3$

It is interesting to compare $ScF_3$ with the isostructural compound $ReO_3$. At ambient pressure, $ReO_3$ exhibits a perovskite $c$-lattice structure from the lowest observed temperature up to its melting point, despite its empty $A$ site and therefore low tolerance factor [3]. The stability of the $c$ phase is a consequence of its metallicity: the Fermi pressure of delocalized Re $5d$ electrons that occupy the $\pi^*$ conduction band keep the $ReO_6$ octahedra from tilting [42]. On the other hand, such states are empty in the wide-gap insulator $ScF_3$

TABLE II. Transition temperatures ($T_c$), isothermal entropy changes ($\Delta S$), isothermal heats ($\mathcal{Q} = T_c \Delta S$), pressure changes ($\Delta P$), caloric strengths ($\Delta S/\Delta P$), refrigerant capacity (RC), and $T - P$ slope ($dT_c/dP$) of giant barocaloric materials.

| Compound | $T_c$ [K] | $\Delta S$ [J K$^{-1}$ kg$^{-1}$] | $\mathcal{Q}$ [kJ kg$^{-1}$] | $\Delta P$ [GPa] | $\frac{\Delta S}{\Delta P}$ [J K$^{-1}$ kg$^{-1}$ GPa$^{-1}$] | RC [J kg$^{-1}$] | $\frac{dT_c}{dP}$ [K GPa$^{-1}$] | Ref. |
|---|---|---|---|---|---|---|---|---|
| $Ni_{49.26}Mn_{36.08}In_{14.66}$ | 293 | 24 | 7.0 | 0.26 | 92 | 120 | 18 | [28] |
| $LaFe_{11.33}Co_{0.47}Si_{1.2}$ | 237 | 8.7 | 2.0 | 0.20 | 43.5 | 81 | 73 | [29] |
| $(NH_4)_3MoO_3F_3$ | 297 | 55 | 16.3 | 0.5 | 110 | 5200 | 202 | [30] |
| $Gd_5Si_2Ge_2$ | 270 | 11 | 2.9 | 0.20 | 55 | 180 | 32 | [31] |
| $Fe_{49}Rh_{51}$ | 308 | 12.5 | 3.8 | 0.11 | 114 | 105 | 54 | [32] |
| $Mn_3GaN$ | 285 | 21.6 | 6.2 | 0.09 | 240 | 125 | 65 | [33] |
| $(NH_4)_2SO_4$ | 219 | 60 | 13.2 | 0.10 | 600 | 276 | 45 | [34] |
| $BaTiO_3$ | 400 | 1.6 | 0.64 | 0.10 | 16 | 10 | −58 | [35] |
| [TPrA] [Mn(dca)$_3$] | 330 | 35.1 | 11.6 | 0.00689 | 5094 | 62 | 231 | [36] |
| $Sc_{1-x}Ti_xF_3$ ($x = 0.85$) | 283 | 12 | 3.4 | 0.10 | 120 | 406 | 723 | This work |

[18]. Its lattice structure remains cubic at all temperatures due to its purely ionic Madelung energy [14]. Both compounds exhibit incipient lattice instabilities in their $c$ phases. In $ScF_3$, softening of the entire $M$-$R$ phonon branch (with the lowest point at $R$) has been observed by IXS [19] from 300 to 8 K at ambient pressure and also found by a first-principles calculation [20]. The temperature dependence of the phonon energies is well described by mean-field theory, as discussed above. Condensation of the $R_4^+$ mode and its associated $c$-$r$ transition can be induced by modest hydrostatic compression (∼0.6 GPa at RT) [21,23,24] or cation substitution [4,5,7]. It is unknown whether the transition is of first or second order. In $ReO_3$, inelastic neutron scattering experiments [43] (INS) have observed softening from 280 to 2 K without condensation of the $M_3^+$ phonon mode, which consists of in-phase rotations of rigid $ReO_6$ octahedra along a [100] axis that passes through the metal cation. The supposedly observed linear temperature dependence of the mode energy is unusual, as it is shown by the blue dashed line in Fig. 6. However, we make the observation that the linear fit is hardly distinguishable from the standard mean-field behavior, $\omega_{M_3^+} \propto \sqrt{A_0(T - T_0)}$, with physically reasonable parameters ($A_0 \simeq 2.5 \times 10^{-3}$ meV K$^{-1}$ Å$^{-5}$, and $T_0 \simeq -296$ K); see solid red line in Fig. 6. The mode can be condensed upon application of moderate pressures (∼0.5 GPa at RT), and a $P - T$ phase diagram has been established by neutron diffraction experiments [44] in which the high-pressure phase has $c$ symmetry ($Im3$) and the transition line is of second order [45]. A recent first-principles calculation [46] has suggested that the $c$-$c$ transition is weakly first order. Additional pressure-induced transitions have been reported in $ScF_3$ [23,24] and $ReO_3$ [47] at higher pressures.

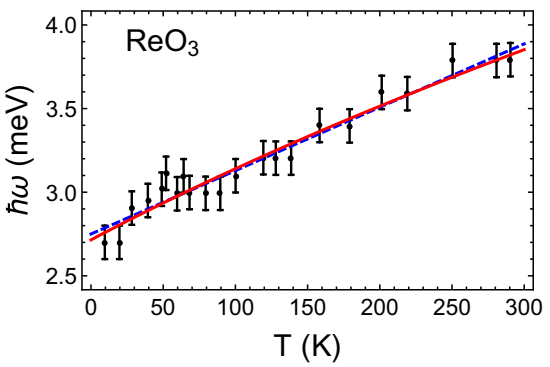


FIG. 6. Temperature dependence of the $M_3^+$ phonon mode in $ReO_3$. Dashed-blue and solid-red lines correspond to purely linear and classical mean-field behavior, respectively. Data taken from Ref. [43].

Both $ScF_3$ [21] and $ReO_3$ [48–50] exhibit negative TE over a wide temperature range with a common origin: large quartic anharmonicities of their corresponding soft $R_4^+$ and $M_3^+$ modes consisting of rigid antiphase rotations of the $ScF_6$ and $ReO_6$ octahedra, respectively [22,43]. The size of the effect, however, is an order of magnitude larger in $ScF_3$ than in $ReO_3$. This can be understood from the distinct nature of their metal-nonmetal bonds. In $ScF_3$, there is little overlap between the charge densities that form the ionic bond between $Sc^{3+}$ and $F^-$ [38], which favors large buckling fluctuations in the Sc-F-Sc chains. In $ReO_3$, the buckling fluctuations of the Re-O-Re bonds are reduced by the stiffer covalent bond formed by hybridized Re 5$d$ and O 2$p$ electrons [42,51].

### D. Comparison to $WO_3$

Another interesting compound to compare with is tungsten bronze $WO_3$. Like $ScF_3$, $WO_3$ is an insulator but its high-temperature phase is tetragonal ($t$) and it goes through several structural transitions upon cooling [3]. Its hypothetical $c$ structure has an unstable $M_3^-$ mode consisting of opposite displacements of the cations and anions from unit cell to unit cell along the [110] directions [52], which generate off-center displacements of $W^{6+}$ towards one of its nearest $O^{2-}$ with concomitant increase in their covalency [53]. Condensation of this mode leads to a $t$ structure of highly distorted $WO_6$ octahedra [54]. The energy gain due to the increase in covalency between $W^{6+}$ and $O^{2-}$ favors the $t$ phase over the ionic $c$ structure [53]. The $c$ phase can be stabilized in $WO_3$ by introducing electrons: when doped with Na, 3$s$ electrons begin to occupy the conduction band and, for sufficiently large concentrations, their Fermi pressure stabilizes the $c$ phase [51]. Such a $c$ phase displays PTE and mean-field softening with temperature of its $M_3^-$ phonon mode down to about 416 K, where a structural transition to a $t$ phase occurs [55].

## IV. CONCLUSIONS

We have presented a Landau theory for trifluoride and have used it to calculate and predict the temperature and

pressure dependence of several thermodynamic quantities. We have compared our results to existing experimental data on trifluorides and have quantified the deviations from mean-field theory. We have found that the fluctuations of their rigid $MF_6$ octahedra tend to increase with the metal cation size. We have used our model to predict a giant BCE in $Sc_{1-x}Ti_xF_3$ ($x = 0.85$) of up to $15\,J\,K^{-1}\,kg^{-1}$ for a pressure change of 0.2 GPa. This effect extends over a temperature range of over 140 K, which includes RT. Our results suggest that open lattice frameworks such as the trifluorides could be a promising platform to search for giant barocaloric effects.

## ACKNOWLEDGMENTS

G.G.G.V. thanks Xavier Moya and Esteban Avedaño for useful discussions and Jason Hancock and Sahan Handunkanda for carefully reading the manuscript. Work at the University of Costa Rica is supported by the Vice Rectory for Research under Project No. 816-B5-220, and work at Argonne National Laboratory is supported by the US Department of Energy, Office of Basic Energy Sciences, Material Sciences and Engineering Division under Contract No. DE-AC02-06CH11357. G.G.G.V. and R.T.B. acknowledge partial financial support from the Office of International Affairs at the University of Costa Rica.

## APPENDIX A: SOFT-MODE FREQUENCIES

The soft-mode frequencies are computed from the free energy (2) with the $\eta's$ constant [26],

$$\varrho(\omega_i)^2\delta_{ij} = \frac{\partial^2(G_Q + G_\eta)}{\partial\hat{Q}_i\partial\hat{Q}_j}, \quad (i,j = 1,2,3), \tag{A1}$$

where $\hat{Q}_i$ are principal-axis coordinates of the soft mode and $\varrho = 2m_F/a^3$ is the mass density of fluorine atoms participating in each mode, where $m_F$ is the mass of the fluorine atom. The soft-mode frequencies given in Eq. (A1) must be evaluated at the equilibrium points given in Eqs. (8) and (4). The free energy $G$ appearing in Eq. (A1) is that of Eq. (2) rather than that of Eq. (5) because the frequency of the acoustic modes associated with uniform strains vanishes in the long-wavelength limit [26].

In the $c$ phase, the frequency of the $R_4^+$ mode is threefold degenerate since all strains vanish:

$$\varrho\,\omega^2_{R_4^+} = \tilde{A}. \tag{A2}$$

In the $r$ phase, the mode splits into the $E_g$ doublet and the $A_{1g}$ singlet,

$$\varrho\,\omega^2_{E_g} = \tilde{A} + \left(2\tilde{u} + 8\frac{e_a^2}{C_a} + 6\frac{e_t^2}{C_t} + \frac{1}{3}\frac{e_r^2}{C_r} + w_1\,Q_s^2\right)Q_s^2, \tag{A3a}$$

$$\varrho\,\omega^2_{A_{1g}} = \tilde{A} + \left(6[\tilde{u} + \tilde{v}] + 28\frac{e_a^2}{C_a} + \frac{4}{3}\frac{e_r^2}{C_r} + 5w_1\,Q_s^2\right)Q_s^2, \tag{A3b}$$

where $Q_s$ is given in Eq. (8).

## APPENDIX B: SIXTH-ORDER $c$ ANISOTROPY

In this Appendix, we discuss the effects of sixth-order anisotropies in some of our previous results. We will show that such anisotropies allow us to describe a possible phase competition between pressure-induced phases. So far, the evidence for phase competition has been experimentally reported in $ScF_3$ [23,24], where near about 3.0 GPa, the $r$ phase destabilizes and a structural transition to an orthorhombic ($o$) phase occurs. In addition, a MD simulation of $AlF_3$ has found a metastable $o$ phase in the free energy at ambient pressure and below the $c$-$r$ transition temperature [16]. No $r$-$o$ transition has been observed in $TiF_3$, $FeF_3$, and $CrF_3$ [56,57].

It is well known that the free energy (5) does not support a stable $o$ phase [25]. To include it, we must add sixth-order $c$ anisotropies,

$$\frac{3w_2}{4}\left[Q_1^2(Q_2^4 + Q_3^4) + Q_2^2(Q_1^4 + Q_3^4) + Q_3^2(Q_1^4 + Q_2^4)\right] + \frac{9w_3}{2}Q_1^2Q_2^2Q_3^2, \tag{B1}$$

where $w_2$ and $w_3$ are parameters independent of temperature and pressure. We consider the following order parameters for the $t$, $o$, and $r$ phases:

$$t : (Q_1,Q_2,Q_3) = Q_s(0,0,1),$$
$$o : (Q_1,Q_2,Q_3) = \frac{Q_s}{\sqrt{2}}(1,1,0),$$
$$r : (Q_1,Q_2,Q_3) = \frac{Q_s}{\sqrt{3}}(1,1,1).$$

The contribution from the anisotropic terms of Eq. (B1) to the free energy is

$$\tilde{G}_{AN}(\mathrm{t}) = 0, \tag{B2a}$$
$$\tilde{G}_{AN}(\mathrm{o}) = \left(\tfrac{3}{8}\tilde{v} + \tfrac{3}{16}w_2Q_s^2\right)Q_s^4, \tag{B2b}$$
$$\tilde{G}_{AN}(\mathrm{r}) = \left(\tfrac{1}{2}\tilde{v} + \tfrac{1}{6}(w_2 + w_3)Q_s^2\right)Q_s^4. \tag{B2c}$$

For simplicity, we take $w_2 = 0$. Then, for $\tilde{v} < 0$ and $w_1 + w_3 > 0$, we find that the $r$ phase is the global minimum for small spontaneous distortions $[Q_s^2 < -(3/4)(\tilde{v}/w_3)]$ while the $o$ phase is a local minimum; and vice versa for large distortions $[Q_s^2 > -(3/4)(\tilde{v}/w_3)]$. For $\tilde{v} < 0$ and $w_1 + w_3 \leqslant 0$, the energy has unphysical divergences, implying that higher-order terms must be taken into account. The $t$ phase is always metastable.

The order parameter of the $o$ phase with $w_2 = 0$ is given as follows:

$$Q_s(T,P) = \pm\left\{\sqrt{\left(\frac{\tilde{u} + 3\tilde{v}/4}{w_1}\right)^2 - \frac{\tilde{A}}{w_1}} - \left(\frac{\tilde{u} + 3\tilde{v}/4}{w_1}\right)\right\}^{1/2},$$

where $\tilde{A}$ is given by Eq. (6). The order parameter of the $r$ phase with sixth-order anisotropies is obtained by replacing $w_1 \to w_1 + w_3$ in Eq. (8).

Figure 7(a) shows a generic $w_3 - T$ phase diagram at ambient pressure calculated by comparing the free energies

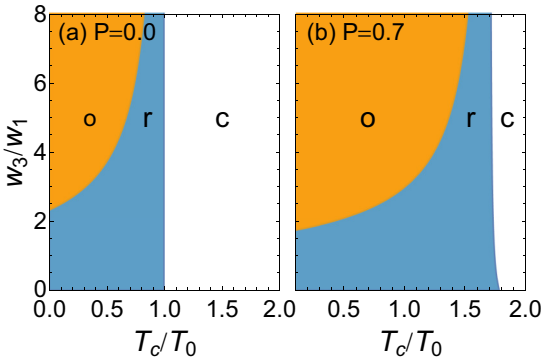


FIG. 7. Schematic phase diagrams of the trifluoride (a) at ambient pressure and (b) with applied hydrostatic compression. All transition lines are of first order. Here, $A_0T_0/(w_1a^4) = 1.0 \times 10^{-3}$, $\tilde{u}/(w_1a^2) = 6.0 \times 10^{-2}$, and $\tilde{v}/(w_1a^2) = -7.0 \times 10^{-2}$. $P$ is in units of $C_aA_0T_0/(2e_a)$.

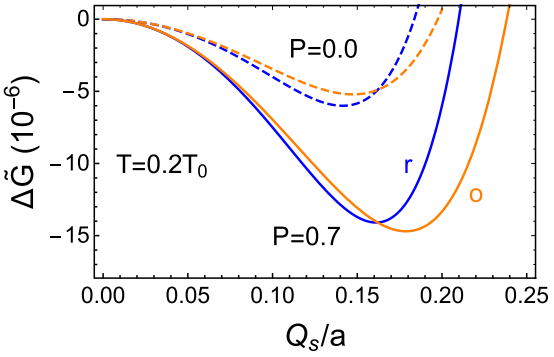


FIG. 8. Free energy densities for $w_3/w_1 = 2.0$. $\Delta\tilde{G}$ and $P$ are in units of $w_1a^6$ and $C_aA_0T_0/(2e_a)$, respectively.

of the $c$, $r$, and $o$ minima. For small anisotropies ($w_3/w_1 \lesssim 2.2$), we find there is only a $c$-$r$ phase transition, while for large anisotropies ($w_3/w_1 \gtrsim 2.2$), an additional $r$-$o$ phase change occurs at low temperatures. Figure 7(b) shows the $w_3 - T$ phase diagram at an applied pressure. As expected, pressure favors ordering as the $c$-$r$ and $r$-$o$ transitions are pushed to higher temperatures. The corresponding free energy changes $\Delta\tilde{G} = \tilde{G} - G_0 + P^2/(2C_a)$ of the $r$ and $o$ phases for $w_3/w_1 = 2.0$ are shown in Fig. 8. The free energy of the metastable $t$ phase is not shown for clarity. At ambient pressure, the $r$ phase is a global minimum while the $o$ phase is metastable, which is in agreement with MD simulations [16]. With large enough applied pressures, the situation reverses and the $r$ phase becomes a local minimum while the $o$ phase is the ground state. Metal trifluorides must then lie in the region of low anisotropy ($w_3/w_1 < 2.2$), as no transition to an $o$ phase has been observed at ambient pressure.


[1] M. A. Hepworth, K. H. Jack, R. D. Peacock, and G. J. Westland, The crystal structures of the trifluorides of iron, cobalt, ruthenium, rhodium, palladium, and iridium, Acta Crystallogr. **10**, 63 (1957).

[2] P. Daniel, A. Bulou, M. Rousseau, J. Nouet, and M. Leblanc, Raman-scattering study of crystallized $MF_3$ compounds (M = Al, Cr, Ga, V, Fe, In): An approach to the short-range-order force constants, Phys. Rev. B **42**, 10545 (1990).

[3] N. Tsuda, K. Nasu, A. Fujimori, and K. Siratori, *Electronic Conduction in Oxides* (Springer, New York, 2000).

[4] C. R. Morelock, B. K. Greve, L. C. Gallington, K. W. Chapman, and A. P. Wilkinson, Negative thermal expansion and compressibility of $Sc_{1-x}Y_xF_3$ ($x \leqslant 0.25$), J. Appl. Phys. **114**, 213501 (2013).

[5] C. R. Morelock, L. C. Gallington, and A. P. Wilkinson, Evolution of negative thermal expansion and phase transitions in $Sc_{1-x}Ti_xF_3$, Chem. Mater. **26**, 1936 (2014).

[6] L. Hu, J. Chen, L. Fan, Y. Ren, Y. Rong, Z. Pan, J. Deng, R. Yu, and X. Xing, Zero thermal expansion and ferromagnetism in cubic $Sc_{1-x}M_xF_3$ (M = Ga, Fe) over a wide temperature range, J. Am. Chem. Soc. **136**, 13566 (2014).

[7] C. R. Morelock, L. C. Gallington, and A. P. Wilkinson, Solid solubility, phase transitions, thermal expansion, and compressibility in $Sc_{1-x}Al_xF_3$, J. Solid State Chem. **222**, 96 (2015).

[8] C. P. Romao, C. R. Morelock, A. P. Wilkinson, and M. Anne, The heat capacities of thermomiotic $ScF_3$ and $ScF_3$-$YF_3$ solid solutions, J. Mater. Sci. **50**, 3409 (2015).

[9] T. Wang, J. Xu, L. Hu, W. Wang, R. Huang, F. Han, Z. Pan, J. Deng, Y. Ren, L. Li, J. Chen, and X. Xing, Tunable thermal expansion and magnetism in Zr-doped $ScF_3$, Appl. Phys. Lett. **109**, 181901 (2016).

[10] J. Chen, Q. Gao, A. Sanson, X. Jiang, Q. Huang, A. Carnera, C. G. Rodriguez, L. Olivi, L. Wang, L. Hu, K. Lin, Y. Ren, Z. Lin, C. Wang, L. Gu, J. Deng, J. P. Attfield, and X. Xing, Tunable thermal expansion in framework materials through redox intercalation, Nat. Commun. **8**, 14441 (2017).

[11] L. Wang, C. Wang, Y. Sun, K. Shi, S. Deng, H. Lu, P. Hu, and X. Zhang, Metal fluorides, A new family of negative thermal expansion materials, J. Materiomics **1**, 106 (2015); J. Chen, L. Hu, J. Deng, and X. Xing, Negative thermal expansion in functional materials: Controllable thermal expansion by chemical modifications, Chem. Soc. Rev. **44**, 3522 (2015); C. P. Romao, K. J. Miller, C. A. Whitman, M. A. White, and B. A. Marinkovic, 4.07–Negative thermal expansion (thermomiotic) materials, in *Comprehensive Inorganic Chemistry II*, edited by J. Reedijk and K. Poeppelmeier, 2nd ed. (Elsevier, Amsterdam, 2013), p. 127; C. Lind, Two decades of negative thermal expansion research: Where do we stand? Materials **5**, 1125 (2012); W. Miller, C. W. Smith, D. S. Mackenzie, and K. E. Evans, Negative thermal expansion: A review, J. Mater. Sci. **44**, 5441 (2009).

[12] C. R. Morelock, J. C. Hancock, and A. P. Wilkinson, Thermal expansion and phase transitions of $\alpha$-$AlF_3$, J. Solid State Chem. **219**, 143 (2014).

[13] B. J. Kennedy and T. Vogt, Powder x-ray diffraction study of the rhombohedral to cubic phase transition in $TiF_3$, Mater. Res. Bull. **37**, 77 (2002).

[14] Y.-R. Chen, V. Perebeinos, and P. B. Allen, Density-functional study of the cubic-to-rhombohedral transition in $\alpha$-$AlF_3$, Phys. Rev. B **69**, 054109 (2004).

[15] P. Daniel, A. Bulou, M. Rousseau, J. Nouet, J. L. Fourquet, M. Leblanc, and R. Burriel, A study of the structural phase transitions in $AlF_3$: X-ray powder diffraction, differential scanning calorimetry (DSC) and Raman scattering investigations of the lattice dynamics and phonon spectrum, J. Phys.: Condens. Matter **2**, 5663 (1990).

[16] S. Chaudhuri, P. J. Chupas, M. Wilson, P. Madden, and C. P. Grey, Study of the nature and mechanism of the rhombohedral-to-cubic phase transition in $\alpha$-$AlF_3$ with molecular dynamics simulations, J. Phys. Chem. B **108**, 3437 (2004).

[17] P. B. Allen, Y.-R. Chen, S. Chaudhuri, and C. P. Grey, Octahedral tilt instability of $ReO_3$-type crystals, Phys. Rev. B **73**, 172102 (2006).

[18] D. Bocharov, P. Žguns, S. Piskunov, A. Kuzmin, and J. Purans, Electronic structure of cubic $ScF_3$ from first-principles calculations, Low Temp. Phys. **42**, 556 (2016); H. B. Hamed, A. Qteish, N. Meskini, and M. Alouani, Calculated hybrid and semilocal functionals and $GW$ electronic structure of the metal trifluorides $MF_3$ ($M$ = Sc, Y, Al), Phys. Rev. B **92**, 165202 (2015).

[19] S. U. Handunkanda, E. B. Curry, V. Voronov, A. H. Said, G. G. Guzmán-Verri, R. T. Brierley, P. B. Littlewood, and J. N. Hancock, Large isotropic negative thermal expansion above a structural quantum phase transition, Phys. Rev. B **92**, 134101 (2015).

[20] A. van Roekeghem, J. Carrete, and N. Mingo, Anomalous thermal conductivity and suppression of negative thermal expansion in $ScF_3$, Phys. Rev. B **94**, 020303 (2016).

[21] B. K. Greve, K. L. Martin, P. L. Lee, P. J. Chupas, K. W. Chapman, and A. P. Wilkinson, Pronounced negative thermal expansion from a simple structure: Cubic $ScF_3$, J. Am. Chem. Soc. **132**, 15496 (2010).

[22] Chen W. Li, Xiaoli Tang, J. A. Muñoz, J. B. Keith, S. J. Tracy, D. L. Abernathy, and B. Fultz, Structural Relationship Between Negative Thermal Expansion and Quartic Anharmonicity of Cubic $ScF_3$, Phys. Rev. Lett. **107**, 195504 (2011).

[23] K. S. Aleksandrov, V. N. Voronov, A. N. Vtyurin, A. S. Krylov, M. S. Molokeev, M. S. Pavlovskiĭ, S. V. Goryaĭnov, A. Yu. Likhacheva, and A. I. Ancharov, Pressure-induced phase transition in the cubic $ScF_3$ crystal, Phys. Solid State **51**, 810 (2009).

[24] K. S. Aleksandrov, V. N. Voronov, A. N. Vtyurin, S. V. Goryainov, N. G. Zamkova, V. I. Zinenko, and A. S. Krylov, Lattice dynamics and hydrostatic-pressure-induced phase transitions in $ScF_3$, J. Exp. Theor. Phys. **94**, 977 (2002).

[25] R. A. Cowley, Structural phase transitions, I. Landau theory, Adv. Phys. **29**, 1 (1980).

[26] J. C. Slonczewski and H. Thomas, Interaction of elastic strain with the structural transition of strontium titanate, Phys. Rev. B **1**, 3599 (1970).

[27] L. Mañosa and A. Planes, Materials with giant mechanocaloric effects: Cooling by strength, Adv. Mater. **29**, 1603607 (2017); B. Lu and J. Liu, Mechanocaloric materials for solid-state cooling, Sci. Bull. **60**, 1638 (2015); X. Moya, S. Kar-Narayan, and N. D. Mathur, Caloric effects near ferroic transitions, Nat. Mater. **13**, 439 (2014).

[28] L. Mañosa, D. González-Alonso, A. Planes, E. Bonnot, M. Barrio, J.-L. Tamarit, S. Aksoy, and M. Acet, Giant solid-state barocaloric effect in the Ni-Mn-In magnetic shape-memory alloy, Nat. Mater. **9**, 478 (2010).

[29] L. Mañosa, D. Gonzáez-Alonso, A. Planes, M. Barrio, J.-L. Tamarit, I. S. Titov, M. Acet, A. Bhattacharyya, and S. Majumdar, Inverse barocaloric effect in the giant magnetocaloric La-Fe-Si-Co compound, Nat. Commun. **2**, 595 (2011).

[30] I. N. Flerov, M. V. Gorev, A. Tressaud, and N. M. Laptash, Perovskite-like fluorides and oxyfluorides: Phase transitions and caloric effects, Crystallogr. Rep. **56**, 9 (2011).

[31] S. Yuce, M. Barrio, B. Emre, E. Stern-Taulats, A. Planes, J.-L. Tamarit, Y. Mudryk, K. A. Gschneidner, Jr., V. K. Pecharsky, and L. Mañosa, Barocaloric effect in the magnetocaloric prototype $Gd_5Si_2Ge_2$, Appl. Phys. Lett. **101**, 071906 (2012).

[32] E. Stern-Taulats, A. Planes, P. Lloveras, M. Barrio, J.-L. Tamarit, S. Pramanick, S. Majumdar, C. Frontera, and L. Mañosa, Barocaloric and magnetocaloric effects in $Fe_{49}Rh_{51}$, Phys. Rev. B **89**, 214105 (2014).

[33] D. Matsunami, A. Fujita, K. Takenaka, and M. Kano, Giant barocaloric effect enhanced by the frustration of the antiferromagnetic phase in $Mn_3GaN$, Nat. Mater. **14**, 73 (2015).

[34] P. Lloveras, E. Stern-Taulats, M. Barrio, J.-Ll. Tamarit, S. Crossley, W. Li, V. Pomjakushin, A. Planes, Ll. Mañosa, N. D. Mathur, and X. Moya, Giant barocaloric effect at low pressure in ferroelectric ammonium sulphate, Nat. Commun. **6**, 8801 (2015).

[35] E. Stern-Taulats, P. Lloveras, M. Barrio, E. Defay, M. Egilmez, A. Planes, J.-L. Tamarit, L. Mañosa, N. D. Mathur, and X. Moya, Inverse barocaloric effects in ferroelectric $BaTiO_3$ ceramics, APL Mater. **4**, 091102 (2016).

[36] J. M. Bermúdez-García, M. Sánchez-Andújar, and S. Castro-García, Giant barocaloric effect in the ferroic organic-inorganic $[TPrA][Mn(dca)_3]$ perovskite under easily accessible pressures hybrid, Nat. Commun. **8**, 15715 (2017).

[37] S. Piskunov, P. A. Žguns, D. Bocharov, A. Kuzmin, J. Purans, A. Kalinko, R. A. Evarestov, S. E. Ali, and F. Rocca, Interpretation of unexpected behavior of infrared absorption spectra of $ScF_3$ beyond the quasiharmonic approximation, Phys. Rev. B **93**, 214101 (2016).

[38] Y. Liu, Z. Wang, M. Wu, Q. Sun, M. Chao, and Y. Jia, Negative thermal expansion in isostructural cubic $ReO_3$ and $ScF_3$: A comparative study, Comput. Mater. Sci. **107**, 157 (2015).

[39] V. I. Zinenko and N. G. Zamkova, Lattice dynamics of $MF_3$ crystals (M = Al, Ga, and In), Phys. Solid State **42**, 1348 (2000).

[40] B. A. Strukov and A. P. Levanyuk, *Ferroelectric Phenomena in Crystals: Physical Foundations* (Springer, New York, 1964).

[41] P. J. Chupas, S. Chaudhuri, J. C. Hanson, X. Qiu, P. L. Lee, S. D. Shastri, S. J. L. Billinge, and C. P. Grey, Probing local and long-range structure simultaneously: An in situ study of the high-temperature phase transition of $\alpha$-$AlF_3$, J. Am. Chem. Soc. **126**, 4756 (2004).

[42] M. G. Stachiotti, F. Corà, C. R. A. Catlow, and C. O. Rodriguez, First-principles investigation of $ReO_3$ and related oxides, Phys. Rev. B **55**, 7508 (1997).

[43] T. Chatterji, P. G. Freeman, M. Jimenez-Ruiz, R. Mittal, and S. L. Chaplot, Pressure- and temperature-induced $M_3$ phonon softening in $ReO_3$, Phys. Rev. B **79**, 184302 (2009).

[44] T. Chatterji and G. J. McIntyre, Pressure-induced structural phase transition in $ReO_3$, Solid State Commun. **139**, 12 (2006).

[45] A recent first-principles calculation [46] has suggested that the c-c transition is weakly first-order.

[46] D. V. S. Muthu, P. Teredesai, S. Saha, Suchitra, U. V. Waghmare, A. K. Sood, and C. N. R. Rao, Pressure-induced structural phase transitions and phonon anomalies in $ReO_3$: Raman and first-principles study, Phys. Rev. B **91**, 224308 (2015).

[47] E. Suzuki, Y. Kobayashi, S. Endo, and T. Kikegawa, Structural phase transition in $ReO_3$ under high pressure, J. Phys.: Condens. Matter **14**, 10589 (2002); J.-E. Jørgensen, J. Staun Olsen, and L. Gerward, Phase transitions in $ReO_3$ studied by high-pressure x-ray diffraction, J. Appl. Crystallogr. **33**, 279 (2000).

[48] E. E. Rodriguez, A. Llobet, T. Proffen, B. C. Melot, R. Seshadri, P. B. Littlewood, and A. C. Cheetham, The role of static disorder in negative thermal expansion in $ReO_3$, J. Appl. Phys. **105**, 114901 (2009).

[49] T. Chatterji, T. C. Hansen, M. Brunelli, and P. F. Henry, Negative thermal expansion of $ReO_3$ in the extended temperature range, Appl. Phys. Lett. **94**, 241902 (2009).

[50] T. Chatterji, P. F. Henry, R. Mittal, and S. L. Chaplot, Negative thermal expansion of $ReO_3$: Neutron diffraction experiments and dynamical lattice calculations, Phys. Rev. B **78**, 134105 (2008).

[51] F. Corà, M. G. Stachiotti, C. R. A. Catlow, and C. O. Rodriguez, Transition metal oxide chemistry: Electronic structure study of $WO_3$, $ReO_3$, and $NaWO_3$, J. Phys. Chem. B **101**, 3945 (1997).

[52] H. Hamdi, E. K. H. Salje, P. Ghosez, and E. Bousquet, First-principles reinvestigation of bulk $WO_3$, Phys. Rev. B **94**, 245124 (2016).

[53] F. Corà, A. Patel, N. M. Harrison, R. Dovesi, and C. R. A. Catlow, An *ab initio* Hartree-Fock study of the cubic and tetragonal phases of bulk tungsten trioxide, J. Am. Chem. Soc. **118**, 12174 (1996).

[54] W. L. Kehl, R. G. Hay, and D. Wahl, The structure of tetragonal tungsten trioxide, J. Appl. Phys. **23**, 212 (1952).

[55] M. Sato, B. H. Grier, G. Shirane, and T. Akahane, Successive structural phase transitions in $Na_xWO_3$, Phys. Rev. B **25**, 6876 (1982).

[56] H. Sowa and H. Ahsbahs, Pressure-induced octahedron strain in $VF_3$-type compounds, Acta Crystallogr., Sect. B: Struct. Sci. **54**, 578 (1998).

[57] J.-E. Jørgensen, W. G. Marshall, and R. I. Smith, The compression mechanism of $CrF_3$, Acta Crystallogr., Sect. B: Struct. Sci. **60**, 669 (2004).